Computers in Biology and Medicine 41 (2011) 483–492

Contents lists available at ScienceDirect

Computers in Biology and Medicine

journal homepage: www.elsevier.com/locate/cbm

Fully automated tumor segmentation based on improved fuzzy connectedness algorithm in brain MR images

Vida Harati [a], Rasoul Khayati [a,*], Abdolreza Farzan [b]

[a] Biomedical Engineering Faculty, Shahed University, Tehran, Iran
[b] Neurosurgery Department, Medical Faculty, Shahed University, Tehran, Iran

ARTICLE INFO

Article history:
Received 26 July 2010
Accepted 25 April 2011

Keywords:
Tumor
Magnetic resonance image
Fuzzy connectedness
Segmentation

ABSTRACT

Uncontrollable and unlimited cell growth leads to tumor genesis in the brain. If brain tumors are not diagnosed early and cured properly, they could cause permanent brain damage or even death to patients. As in all methods of treatments, any information about tumor position and size is important for successful treatment; hence, finding an accurate and a fully automated method to give information to physicians is necessary.

A fully automatic and accurate method for tumor region detection and segmentation in brain magnetic resonance (MR) images is suggested. The presented approach is an improved fuzzy connectedness (FC) algorithm based on a scale in which the seed point is selected automatically. This algorithm is independent of the tumor type in terms of its pixels intensity. Tumor segmentation evaluation results based on similarity criteria (similarity index (*SI*), overlap fraction (*OF*), and extra fraction (*EF*) are 92.89%, 91.75%, and 3.95%, respectively) indicate a higher performance of the proposed approach compared to the conventional methods, especially in MR images, in tumor regions with low contrast. Thus, the suggested method is useful for increasing the ability of automatic estimation of tumor size and position in brain tissues, which provides more accurate investigation of the required surgery, chemotherapy, and radiotherapy procedures.

1. Introduction

Uncontrollable and unlimited cell growth leads to tumor genesis in the brain. Quantitative assessment of the tumors in the brain Magnetic Resonance (MR) images in association with clinical judgment can provide more accurate assessment of the disease progress. Knowledge of the tumor position and size, especially variations in tumor size, can provide important information in order to find out the most effective therapeutic regimes for patients in brain tumor treatments including surgery, radiotherapy, and chemotherapy. The traditional interpretation of MR images by a specialist is a difficult and time-consuming task, and the result directly depends on the experience of the specialist. Also, the complexity and visually vague edges in a number of tumors, and considering the fact that different characteristics of tumor region in images can be obtained even from the same imaging protocols and the noise due to imaging systems, make brain tumor segmentation difficult in a radiologist's manual tracing. Therefore, it is desirable to have an automatic segmentation method to provide an acceptable performance. As a result of this segmentation procedure, the quantitative measure of tumor area (or volume) can be calculated and used for the follow-up of the disease.

There are many proposed approaches, automatic and semi-automatic, for the segmentation of the brain into different tissues, including tumors. These approaches include a variety of methods based on classification using extracted features, level set methods, Markov random field methods, *k*-nearest neighbor (KNN), fuzzy *c*-means, fuzzy connectedness, and region growing [1–7].

Fuzzy clustering techniques based on knowledge and multi-spectral histogram analysis in multifeature space have been applied by Clark et al. [8] for tumor segmentation. In some studies, lesions and tumors have been considered as outliers of a model [8–11]. These methods can show desirable performance when differences between the characteristics of normal and tumor tissues are high. The method proposed by Prastawa et al. [11], which automatically detects tumor tissues, was based on detection of outliers and variations in contrast to that in the normal state. Also, Gering et al. [12] segmented brain tumors by determining image variations in the normal brain via the Markov random field method. Gibbs et al. [13] combined morphological edge detection and the region growing for defining tumor volume, while Kaus et al. [14] used an adaptive template-moderated classification algorithm for MR image classification of five tissue

* Corresponding author. Tel.: +98 21 51212087.
E-mail addresses: khayati@shahed.ac.ir, khayati@aut.ac.ir (R. Khayati).

0010-4825/$ - see front matter © 2011 Elsevier Ltd. All rights reserved.
doi:10.1016/j.compbiomed.2011.04.010

classes, including tumors, whose method is based on an iterative procedure. Taheria et al. [15] introduced a model based on a threshold that used level sets for 3D tumor segmentation. In their model, the level set speed function was designed using a general threshold.

Using fuzzy logic, intelligence has entered into image analysis and processing. Phillips et al. [16] illustrated that intensity distributions of normal tissue and tumor have an overlap, which proved the need to extract more features for tumor segmentation, using a fuzzy clustering concept of brain tumor. Since fuzzy *c*-means clustering is not needed for training data and is independent of the user, it has been extremely used as a clustering method [17–19]. However the method that was recently presented is fuzzy connectedness. Considering that medical images are inherently fuzzy, thus fuzzy connectedness is a very strong tool for medical image processing. Fuzzy connectedness captures togetherness of pixels in the same objective region in spite of gradient variations and inhomogeneity of intensities through the fuzzy process.

The concept of connecting two pixels in an image was called hard fashion (crisp) before 1970, that on the basis of it, pixels were connected or not. Later, for the first time, Rosenfeld [20] introduced the concept of fuzziness by generalizing crisp connectedness to fuzzy subsets. Dellepianeh and Fontana [21], Dellepianeh et al. [22] and Udupa and Samarasekera [23,24] proposed the use of this theory in image segmentation, while the segmentation method proposed by Dellepiane et al. [22] used the connectedness degree of Rosenfeld. As they had defined connectedness strength based on image intensity, their algorithm was sensitive to seed point selection. However, Udupa and Samarasekera [23] proposed a different procedure for fuzzy connectedness and its applications in segmentation. They introduced local fuzzy relation (LFR) or affinity for capturing local togetherness of pixels in image. Through the affinity proposed by Udupa and Samarasekera, different image features were integrated for defining fuzzy connectedness. Subsequently, general fuzzy connectedness (GFC) based on affinity [24] was used for segmentation in combination with the other methods [25–27], especially the deformable model [25,26] methods based on the Voronoi diagram [27] and the level set methods [28]. Moonis et al. [29] studied tumor growth rate after surgery through research for 3D segmentation of tumor based on the theory and principles of fuzzy connectedness. Udupa and Saha [30] calculated volumes of edema and active tumor tissues in FLAIR and T1, respectively, with gadolinium injection by general fuzzy connectedness. Later, the previous segmentation algorithms evolved based on the fuzzy connectedness theory of Pedenkar and Kakadiaris [31]. They used the fuzzy connectedness principles that were a linear composition of components based on homogeneity and objective features with constant weights and then introduced a new method of fuzzy connectedness with dynamic weights (DyW). Hong et al. [32] used the fuzzy connectedness method for displaying tumor surgery procedure. In their method, seed point selection, fuzzy image thresholding, and rectangular selection were carried out by user to reduce the processing time.

Considering the extensive applications of general fuzzy connectedness in image segmentation, the algorithm can also be mistaken for weak region boundaries. However, many fuzzy connectedness algorithms of tumor segmentation showed that human error was involved in the decision and also processing speed, which is dependent on the time of user interaction. What was followed by this research is a fully automatic segmentation procedure, which eliminated user interactions in seed point selection and also improved the performance of general fuzzy connectedness. In the proposed method, the fuzzy behavior of topological and morphological concepts is expanded directly on the desired image and the segmentation procedure is performed.

The article is structured as follows. In Section 2, dataset is introduced and then the proposed method for fully automated tumor segmentation is illustrated in three levels. In the end of this section, evaluation of results is presented. Results of the proposed approach are introduced in Section 3. In Section 4, results and future works are discussed.

Table 1
Position and type of tumors in datasets [33,34].

Main slice #	Location	Intensity level	Tumor	Case
44	Left frontal	High	Meningioma	1
58	Left parasellar	High	Meningioma	2
78	Right parietal	Low	Meningioma	3
35	Left frontal	Low	Low grade glioma	4
92	Right frontal	Low	Astrocytoma	5
81	Right frontal	Low	Low grade glioma	6
92	Right frontal	Low	Astrocytoma	7
39	Left temporal	Low	Astrocytoma	8
31	Left frontotemporal	High	Astrocytoma	9
35	Left temporal	Low	Low grade glioma	10

2. Methods and materials

2.1. Dataset

The proposed procedure in this research was implemented on MR images that were captured from 10 brain tumor patients. This dataset included 124 images with 256×256 resolution for each patient. Slice gap in MR imaging system, size of each pixel in image, and acquisition information were 1.5 mm, 0.9375×0.9375 mm^2, and SPRG[1] T1 POST GAD, respectively [33,34]. After sifting through all the images related to a patient, only tumor images were studied. In this research, the neurologist was asked to perform a manual segmentation of tumors in the MR images of all 10 cases. The results of this manual segmentation provided binary segmented images to the authors for use in evaluation. The position and the type of tumor in the brain and the main slice number are listed in Table 1.

A global framework for this fully automated tumor segmentation method in accordance with the block diagram shown in Fig. 1 is as follows:

- Preprocessing,
- automatic seed point selection,
- tumor segmentation with improved fuzzy connectedness algorithm.

First, the image to enter next steps is preprocessed. Preprocessing consists of two substeps: scale and background noise rejection. Second, seed point that is required for implementation of the fuzzy connectedness algorithm is automatically selected in the tumor region of the image. This step is done by formulization of the tumor region characteristics. Finally, the tumor tissue is segmented using an improved fuzzy connectedness algorithm.

2.2. Preprocessing

As background noise led to errors in the automatic seed point selection algorithm, an anisotropic diffusion filter was used to make a head mask to eliminate this noise [35]. In this filter, by defining a diffusion constant related to the absolute value of the noise gradient and smoothing the background noise by filtering, an appropriate threshold can easily be chosen [36]. For this

[1] Spoiled Gradient Recalled Acquisition.

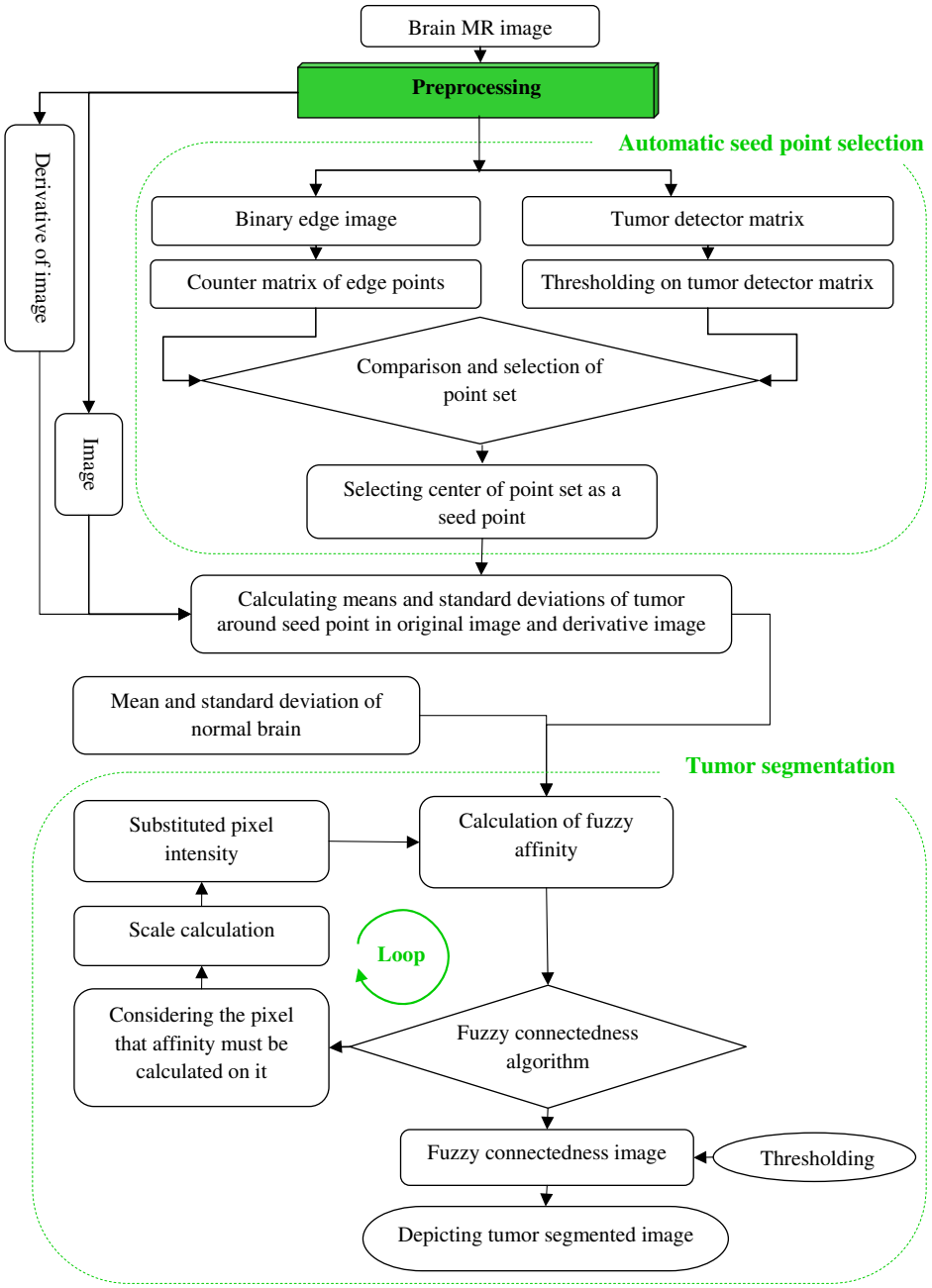

Fig. 1. Block diagram of tumor segmentation by improved fuzzy connectedness algorithm.

purpose, a slightly higher diffusion constant value is considered rather than the absolute value of the noise intensity gradient in its edge. Therefore, a head mask was constructed by thresholding the filtered image. We have studied the dataset of several different images of the brain tumor and have noticed that through trial and error the threshold suitable for those images is within 0.75–0.9; thus we have come to the conclusion that if a constant threshold for all images equal to 0.8 is used, one can obtain good results. Then, for matching intensity ranges in all the images, the highest and the lowest intensities are limited to the interval [0,255].

2.3. *Automatic seed point selection*

The need to do seed point selection within the tumor region to start the fuzzy connectedness algorithm is one of the problems that this algorithm has always faced. Hence, an operator that permanently follows the segmentation procedure is often seen in the articles that used fuzzy connectedness algorithm for segmentation. Thus, this method has been proposed for automatic seed point selection by studying how the tumor is in appearance.

Because of disparity in the tissues that form tumor regions and the amount of blood supply in tumors, even within the same MR imaging protocol, tumors appear with different intensities. So, intensity is not an adequate parameter to achieve the position of the seed point alone. However, one of the characteristics in MR images is that tumors appear with lower or higher intensities than normal brain tissue intensity. Therefore, this characteristic can be used as a feature of tumor tissue. On the other hand, different factors such as placement of living tissue, dead tissue, and tissue calcium together and also the blood vessels in tumor tissue cause inhomogeneity in the tumor region of the image. However, despite these inhomogeneities, some parts always exist

that have considerable homogeneity in the tumor region compared to the normal brain tissue. Hence, considering the local homogeneity of tumor tissue and regardless of the intensity variations in different tumors, differences in tumor intensities with a mean value of tumor area are minimal. Thus, this feature can be another characteristic to determine the position of seed point (second characteristic).

In addition to using these two characteristics in the seed point selection procedure, another feature in the tumor region is considered for increasing the accuracy of the proposed method. Because in homogeneous parts of the tumor tissue, i.e., the region considered for seed point selection, intensity differences are low, the possibility of edge points in this section is very small. Therefore, counting the number of edge points around each pixel with radius R is used as another feature in seed point selection.

Proper formulation of these characteristics, which has been described in six steps, leads to automatic selection of the seed point.

1. Defining tumor detector matrix: this matrix is obtained by applying a tumor detector function on pixels that are the output of the preprocessing step. The tumor detector function has been designed so that the two tumor characteristics described earlier are included (the two characteristics being different tumor tissue intensity from normal brain tissue and local homogeneity of tumor tissue).
   A Gaussian variable coefficient is used in this function to indicate the first characteristic. Through the study of intensities of various tumors in several images, one can conclude that the intensity of the tumor regions is either higher or lower than the intensity of the normal tissues. Therefore, we have chosen a specific function that can, in either case, make the tumor regions be at a lower level intensity with respect to the normal tissues. Thus, we have used a Gaussian function in which the center is the mean of the normal brain tissue intensities. As a result, tumor pixels, after applying this function, appear with low intensity and we can now select the seed point in this region. The Gaussian variable coefficient $\alpha_{Gaussian}(x,y)$ for the point located at x and y coordinates is calculated from
   $$\alpha_{Gaussian}(x,y) = k_1 e^{-(\mu_R-\mu_b)^2/2\sigma_b^2} \quad (1)$$
   In this equation, k_1 is a constant coefficient, μ_R is the mean of intensities in the original image around the point considered with radius R, and μ_b and σ_b are the mean and the standard deviation of intensities in the normal brain tissue, respectively. Also, R is less than the approximated tumor size. For an eye to recognize a tumor, at least 10 pixels are usually required. As such, we have considered the tumor radius to be of 10 pixel size. Tumor detector function is illustrated in Eq. (2), where the neighborhood of each point with radius R in the original image is considered as a neighborhood matrix I_N:$R\times R$. Also, this function includes a logarithmic statement to enter the second characteristic of tumor tissues. Considering the local homogeneity of tumor tissues, one can say that the differences in tumor intensities with a mean value of tumor area are minimal. Thus, to determine the position of the seed point a log function, due to its nonlinear behavior, is a better response to minimize these differences in tumor area:
   $$M_T(x,y) = \alpha_{Gaussian}(x,y)\frac{\log\left(\sum_{i=1}^{R}\sum_{j=1}^{R}|I_N(i,j)-\mu_n|\right)}{\log(R)} \quad (2)$$
   By applying this function, tumor points appear as minimum intensity points in tumor detector matrix; so by thresholding on tumor detector matrix, a point set is achieved in the tumor tissue region.
2. Thresholding on tumor detector matrix: in this algorithm, the threshold to apply the tumor detector matrix is dependent on some parameters such as minimum and maximum of the tumor detector matrix and the total mean of images and also the neighborhood radius R. This threshold is calculated from
   $$Tr = \Gamma_1(\min(M_T)-\max(M_T))+\Gamma_2 R+\Gamma_3\mu \quad (3)$$
   where Γ_1, Γ_2, and Γ_3 are the constant coefficients and μ is the total mean of images. These values are considered constant for all the processed images.
3. Calculating the edge image: for making counter matrix of edge points, an accurate edge detection of image is done by Canny algorithm [37].
4. Forming counter matrix of edge points: in this part, the third characteristic, i.e., the existence of minimum edge points in the homogeneous tumor region, is used. For this purpose, the counter matrix of edge points is made where each value is equal to an edge point number around that point with radius R. Therefore, this value is assigned to each point corresponding to original image points.
5. Comparison and selection of point set: as the number of edge points in the regions with local homogeneity is minimal, in this step, the points that were incorrectly selected are removed via comparison between the tumor detector and the edge counter matrices.
6. Selecting center of point set as seed point: center of point set (obtained from the previous step) is selected as the final seed point.

2.4. Tumor segmentation by improved fuzzy connectedness algorithm

Fuzzy connectedness algorithm used in this study is based on the improvement of the general fuzzy connectedness method [24]. As general fuzzy connectedness algorithm loses its path in the weak boundaries of the same objective region, it enters a new region; thus, this algorithm will be mistaken in these boundaries. Therefore, this approach, by entering appropriate gradient information to the affinity function, has tried to improve algorithm robustness over the boundaries, particularly, over boundaries with lower contrast. On the other hand, affinity is the local concept, and using intensity individually in calculations increases sensitivity of the algorithm with respect to noise. So, for solving these two problems, substituted pixel intensity is applied in all calculations. In each pixel c from the original image, the substituted pixel intensity $I_s(c)$ is defined as

$$I_s(c) = \text{mean}(I(a))_{a\in \text{scale circle}} + \text{mean}(I_{dif}(a))_{a\in \text{scale circle}} \quad (4)$$

In this equation, I and I_{dif} are the original image intensity and the derivative of the original image, respectively. For defining substituted pixel intensity, the means of intensities in these two images in the circle with scale radius around pixel c are calculated. Objective scale in C image around each $c\in C$ element is the biggest circle radius $r(c)$ with center c that is placed completely in the same objective region [38]. Objective scale related to objective region in each pixel has been estimated based on the homogeneous continuity of intensity as described in [38].

In this method, defining more accurate mean and standard deviation values in the objective and nonobjective regions is effective for guiding toward the optimum segmentation method. As the mean and standard deviation values in nonobjective regions mostly change in a small range, these values are used as constant in this algorithm.

Due to a variety of tumor appearances in the image of each patient the mean and the standard deviation of the intensities in the tumor regions are different. In order to calculate such

parameters, each time the seed point is selected automatically, one can consider a circle with radius R around this seed point, in which the objective values are calculated within this circle. This process makes the segmentation algorithm independent of the tumor type with respect to its pixels intensity.

In this algorithm, after calculating the mean and the standard deviation of the tumor region around the seed point, and starting from the seed point, the scale is defined for each pixel and then the substituted pixel (SP) value is calculated to execute an improved fuzzy connectedness algorithm. So, membership strength (affinity) is assigned to each SP based on comparing similarity of SP with tumor region features. This process is repeated for all pixels inside the head mask. Finally, a proper threshold is selected in this algorithm for tumor segmentation (see block diagram shown in Fig. 1).

For implementation of the improved fuzzy connectedness algorithm, adjacency and fuzzy affinity must be defined. In images, adjacency of two pixels c and d, $\mu_\alpha(c,d)$, is defined as

$$\mu_\alpha(c,d)=\begin{cases}1 & \text{if } \sqrt{\sum_i (c_i-d_i)^2}\le 1\\ 0 & \text{otherwise}\end{cases} \tag{5}$$

Also, fuzzy affinity for any two pixels c and d of the image can be expressed as

$$\mu_k(c,d)=\begin{cases}\mu_\alpha(c,d)[w_1h_1(f(c),f(d))+w_2h_2(f(c),f(d))] & \text{if } c\neq d\\ \mu_k(c,d) & \text{if } c=d\end{cases} \tag{6}$$

where $f(c)$ and $f(d)$ are the substituted pixel values in pixels c and d, respectively, and w_1 and w_2 are the weights. Eq. (7) should be established for them [24].

$$w_1+w_2=1 \tag{7}$$

Functional formulations used for h_1 and h_2 are given as Eqs. (8) and (9), respectively. In these two equations, the exponential function argument is normalized by $\max(I)$:

$$h_1(f(c),f(d))=\exp-\left(\left(\frac{1}{2\times\max(I)}\right)\times\left(\frac{((f(c)+f(d))/2)-m_1}{s_1}\right)^2\right) \tag{8}$$

$$h_2(f(c),f(d))=\exp-\left(\left(\frac{1}{2\times\max(I)}\right)\times\left(\frac{((|f(c)-f(d)|)/2)-m_2}{s_2}\right)^2\right) \tag{9}$$

I is an entered image, m_1 and m_2 are the means and s_1 and s_2 are the standard deviations of pixel and absolute values of the image derivative in the objective region, respectively.

With the described formulation, the fuzzy connectedness algorithm through the substituted pixel value segments a more accurate tumor region from other regions in the image. We have used a threshold for the fuzzy connectedness segmentation algorithm by employing the equation, $T_{rF}=0.35(\max(I)-\min(I))$, in which I is the fuzzy connectedness image in our program.

2.5. Evaluation

In this research, criteria including similarity index (*SI*) [39], overlap fraction (*OF*), and extra fraction (*EF*) [40] are used for evaluation. *SI* is a criterion for the correctly segmented region relative to the total segmented region, in both the manual segmentation and the segmented image by the proposed method. The *OF* and the *EF* specify the areas that have been correctly and falsely classified as tumor area, respectively, relative to the tumor area in manual segmentation. Similarity index, overlap fraction, and extra fraction are obtained, respectively, by Eqs. (10), (11), and (12) (see Fig. 2):

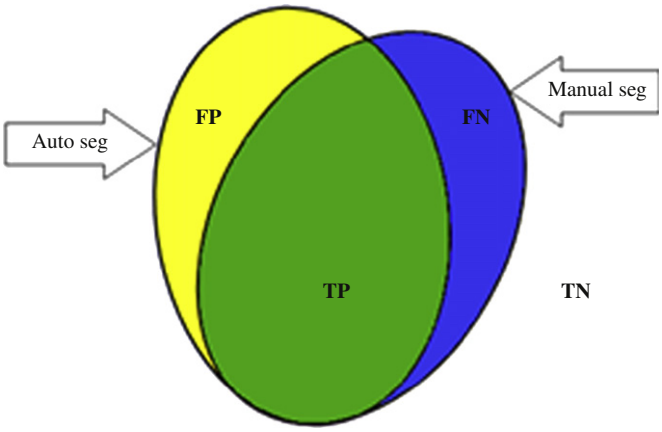

Fig. 2. *TP*, *TF*, *FP*, and *TN* values are shown based on comparison between segmented regions by proposed method (auto seg.) and manual segmentation (manual seg.).

$$SI=\frac{2TP}{2TP+FP+FN} \tag{10}$$

$$OF=\frac{TP}{TP+FN} \tag{11}$$

$$EF=\frac{FP}{TP+FN} \tag{12}$$

In these equations, *TP* is the number of true-positive pixels detected correctly by the method, *FP* is the number of false-positive pixels detected falsely by the method, and *FN* is the number of false-negative pixels relative to the tumor region with manual segmentation but not selected by the method.

In a good segmentation, *SI* and *OF* should be close to 1 and *EF* should be close to 0. Practically, a value for *SI* more than 0.7 represented a very good segmentation [42].

3. Results

The total process that is proposed in this study has been implemented on a dataset, including MR images of 10 patients with brain tumors, using a Pentium 4 (3.2 GHz) processor with 1 GB RAM. The average time needed to automatically select the seed point and the time for performance of the tumor segmentation algorithm are 30 s and 2 min, respectively. To evaluate the represented method, as will be mentioned later, manual segmentation of each image was performed by the neurologist.

To investigate the automatic seed point selection algorithm, this algorithm was implemented on 150 images including tumor in 139 cases; seed points were selected properly and only in 11 cases there were wrong choices. Fig. 3 shows steps of automatic seed point selection in the image including the tumor. The tumor detector image and the edge image, shown in (b) and (c), respectively, are constructed from the original image shown in (a). After applying a threshold on the tumor detector image, the binary image in (d) is obtained, which illustrates the area with low value. Parallel to this thresholding, edge point counter matrix, which is shown in (e), from the edge image is calculated. By comparing the binary image resulting from thresholding and edge points counter image, the point set relative to the tumor region (illustrated in green in (f)) is achieved. Then, the center of this point set is selected as the final seed point for the beginning of the segmentation algorithm shown in (g).

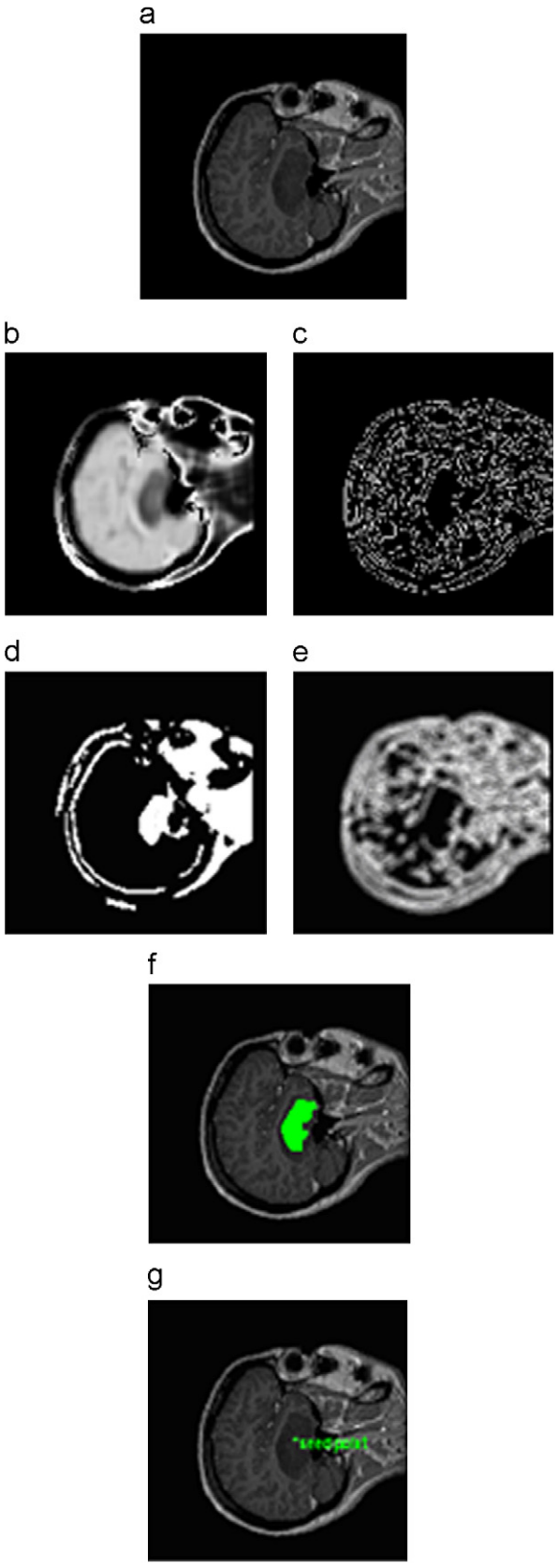

Fig. 3. Results of implementing automatic seed point selection algorithm: (a) input image to automatic seed point selection algorithm, (b) tumor detector matrix, (c) edge points image by applying Canny method, (d) image resulting by thresholding on the tumor detector matrix, (e) edge points counter image, (f) point set obtained from comparison, and (g) final seed point that is considered as the center of point set. (For interpretation of the references to color in this figure, the reader is referred to the web version of this article.)

Results of executing the proposed segmentation approach on two images of patients with two different types of tumor in terms of intensity and image contrast of tumor region are shown in Figs. 4 and 5, which show implementations of the method on MR images corresponding to slice 44 from patient 1 and slice 81 from patient 6. In these two images, (a) is the input image, (b) is the head mask created by an anisotropic filter, (c) is the edge point counter matrix, (d) is the tumor detector matrix, and (e) and (f) are the final results of executing the automatic seed point selection algorithm. Then, the final seed point is calculated as a center of point set and (g) shows the final result of the proposed segmentation approach where manual segmentation is indicated in the left corner of the figure.

To evaluate the accuracy and robustness of the proposed segmentation algorithm, the means of criteria (*SI*, *OF*, and *EF*) related to implementing this method on 10 image sets for 10 patients including brain tumor have been calculated. Mean values of these similarity criteria are given in Table 2 for each patient dataset separately and for all images in the dataset (last line of Table 2).

As seen in Table 2, since good values for the similarity criteria related to the segmented tumors in nearly all images of the datasets are obtained, the proposed algorithm has a high performance. However, it only fails to work so well for the image set 5. In this image set, there are tumors in the sequences of the slices that are surrounded by tissues, which are becoming tumors leading to vague borders for the tumors with very low contrast as compared to the normal tissues. Such tumors are not segmented well in the fully automated segmentation method; therefore, the false-negative results increase and lead to the lower *SI* and *OF*, compared with the other image sets. In spite of a decrease in the *SI* value, as this value is still higher than 0.7, the performance of the proposed algorithm is acceptable [42].

4. Discussion

Representing the fuzzy connectedness theory in image processing by Rosenfeld [20] and especially using it in image segmentation has been an important stage in medical image processing studies. Because of the small differences between image characteristics of various tissues especially adjacent tissues and similarity in some characteristics, tissue segmentation had often been a challenging problem. Based on recent researches in medical image segmentation, the somewhat fuzzy connectedness algorithm has been able to solve problems of medical image segmentation. On the other hand, due to the ability of adaptation in fuzzy connectedness, there is the possibility of proper variations in the fuzzy connectedness algorithm to obtain optimal results in image processing. Almost all the recent algorithms in the field of fuzzy connectedness have used the principles of the algorithm, which was published in 1996 [24]. We have tried to do the same thing, i.e. improving the fuzzy connectedness algorithm of that paper and trying to achieve the desired goal.

Fully automated procedure can be useful in some medical procedures such as robot surgeries that are synchronic with imaging. One of the problems that the fuzzy connectedness algorithm has always been facing is that there is a need for manual seed point selection within the tumor region. Hence, an operator that permanently follows the segmentation procedure is often seen in the articles that used the fuzzy connectedness algorithm for segmentation. Thus, in the present article, we have tried to propose a method for automatic seed point selection that is necessary for algorithm to become fully automatic. This proposed procedure does not affect the accuracy of segmentation. In this study, the improved fuzzy connectedness algorithm for tumor segmentation is started from a seed point that is selected

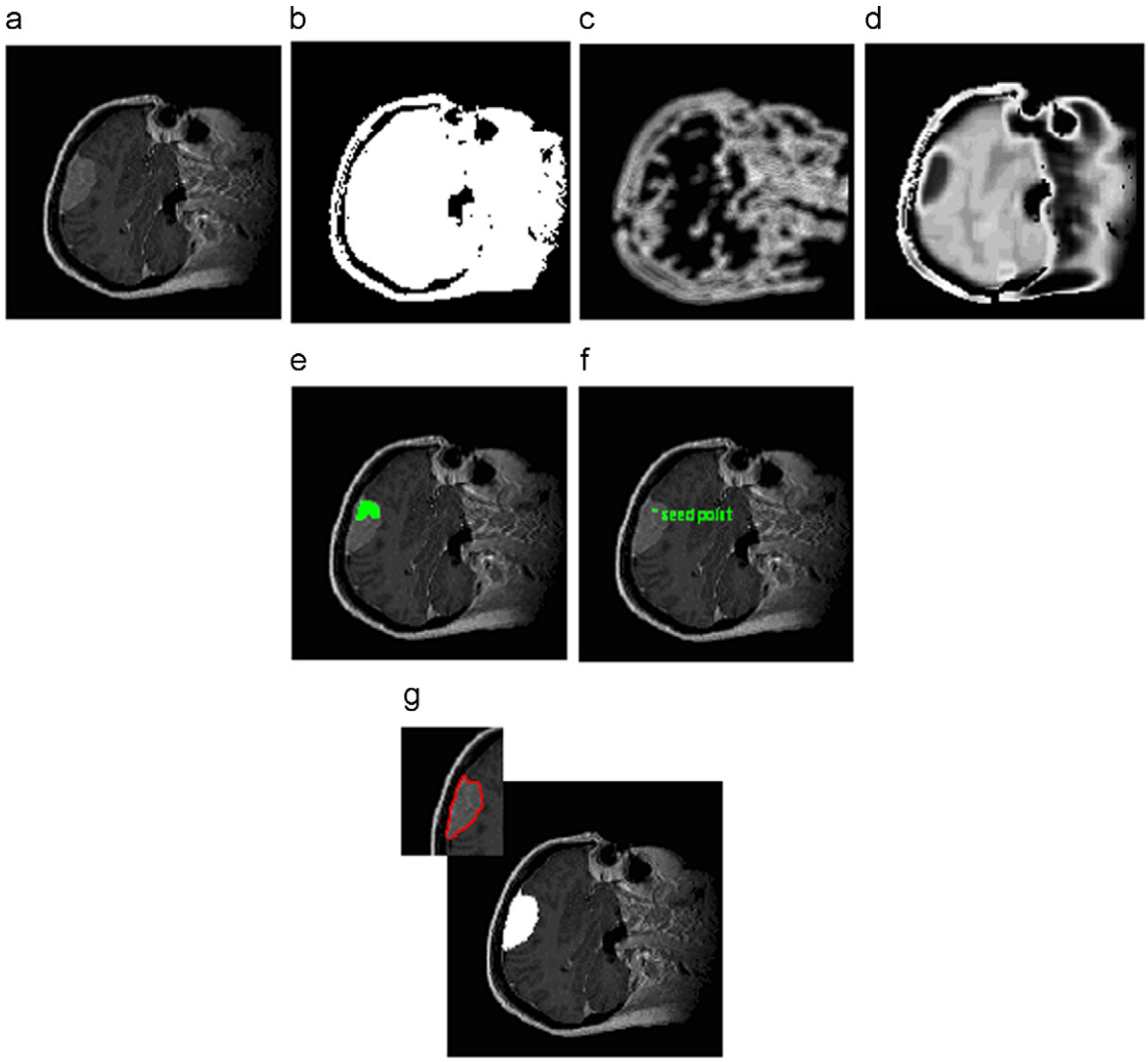

Fig. 4. Representing performance steps of fully automated tumor segmentation by improved fuzzy connectedness algorithm on the image including tumor with high pixel intensity: (a) input image, (b) head mask image, (c) edge points counter image, (d) tumor detector image, (e) seed point set that are selected, (f) final seed point, and (g) result of segmentation by proposed approach (manual segmentation is shown by the red lines in the left corner of (g)). (For interpretation of the references to color in this figure legend, the reader is referred to the web version of this article.)

by automatic seed point selection algorithm. The automatic seed point selection algorithm has been designed on considering the three characteristics of the tumor regions in the image. Using the tumor detector function similar to the tumor segmentation algorithm, this algorithm worked independent of the tumor type with respect to its pixels intensity. Most number of errors in the suggested method for seed point selection occurred in the slices in which the size of tumor is small.

In the proposed tumor segmentation approach, several changes in the implementation of the fuzzy connectedness algorithm have been made. These changes are as follows: first, with regard to the direct relation between fuzzy connectedness and affinity by proper selection of affinity formulation, segmentation results proceeded to better tumor segmentation; second, by fuzzy connectedness concept based on the information related to pixels around the original pixel with radius R instead of fuzzy connectedness based on one pixel, algorithm sensitivity to noise was decreased; and third, by entering extra information such as boundary information of the tumor tissue in the segmentation algorithm, error is reduced.

The improved fuzzy connectedness algorithm, by calculating scale as a homogeneity region radius, used substituted pixel instead of original pixel where the value of the former is obtained by means of intensities and their differences in scale region. The substituted pixel brings boundary information directly into the affinity calculations, so the method presented in this research shows good performance for finding boundaries, especially weak boundaries, with regard to the general fuzzy connectedness algorithm. Comparison between the results of the proposed approach and the general fuzzy connectedness algorithm [24] shows that the fully automatic proposed approach in image segmentation has a high accuracy due to improved changes in the general fuzzy connectedness. Since, the presented method, in which a circle is considered around the seed point, extracts tumor features and uses them in tumor segmentation for each image, the tumor type in terms of its pixels intensity is not affected in tumor segmentation.

For evaluation, a comparison has been done between the proposed approach and the general fuzzy connectedness represented by Udupa and Samarasekera [24]. For this purpose, the general fuzzy connectedness algorithm has been implemented and performed on 10 image sets corresponding to 10 patients.

To demonstrate the robustness of the proposed algorithm in segmenting tumors by weak boundaries in comparison to general

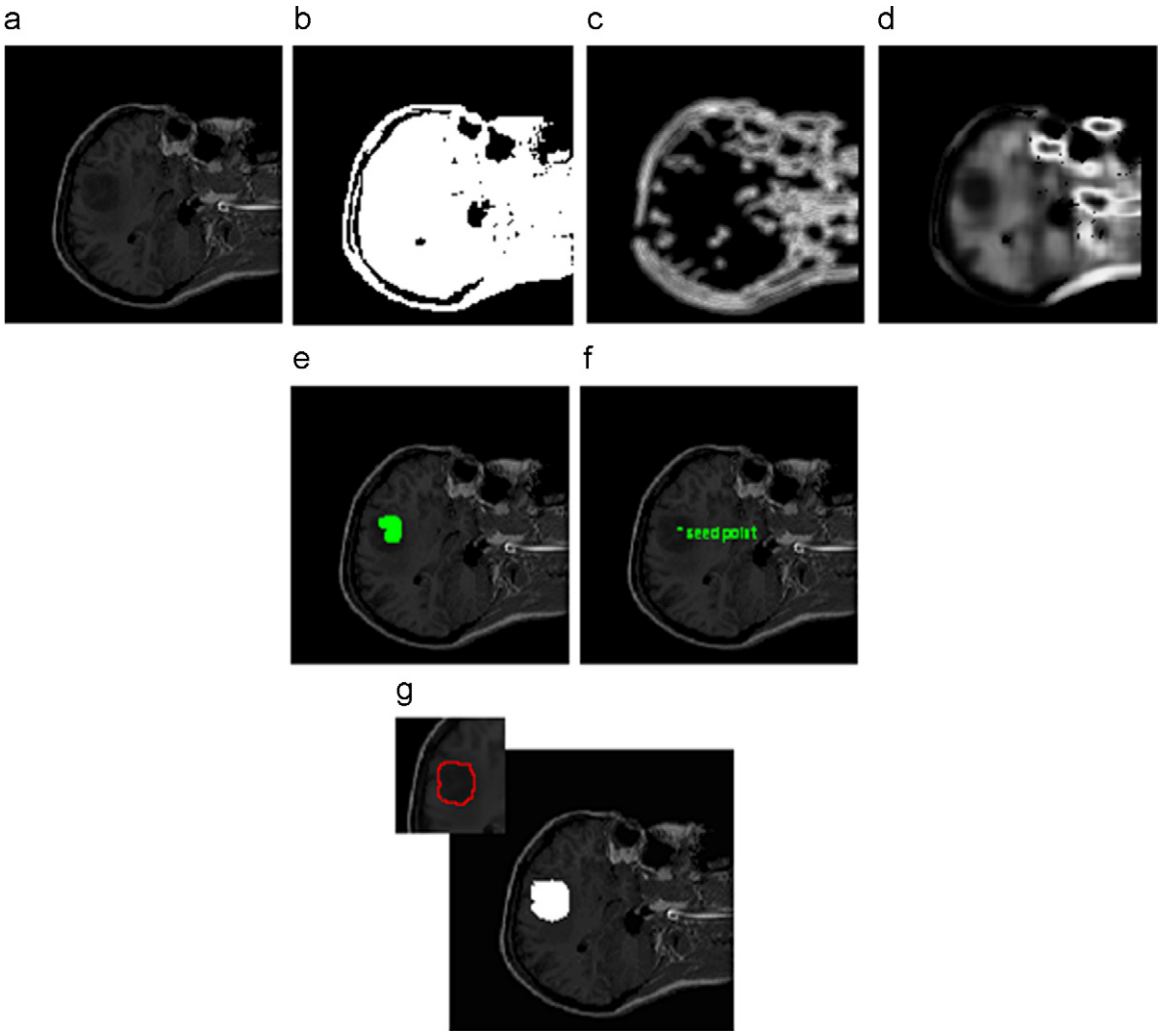

Fig. 5. Representing performance steps of fully automated tumor segmentation by improved fuzzy connectedness algorithm on image including tumor with low pixel intensity: (a) input image, (b) head mask image, (c) edge points counter image, (d) tumor detector image, (e) seed point set that are selected, (f) final seed point, and (g) result of segmentation by proposed approach (manual segmentation is shown by the red lines in the left corner of (g)). (For interpretation of the references to color in this figure legend, the reader is referred to the web version of this article.)

Table 2
Means of criteria, including similarity index (*SI*), overlap fraction (*OF*), and extra fraction (*EF*) for each image set and for the entire image set (end row) resulted from the improved fuzzy connectedness proposed approach.

	SI	*OF*	*EF*
Image set 1	0.985	0.984	0.008
Image set 2	0.90	0.83	0.003
Image set 3	0.981	0.97	0.007
Image set 4	0.98	0.982	0.012
Image set 5	0.71	0.63	0.03
Image set 6	0.99	0.991	0.017
Image set 7	0.993	0.992	0.005
Image set 8	0.96	0.98	0.07
Image set 9	0.81	0.84	0.23
Image set 10	0.98	0.976	0.013
Total means	0.928	0.917	0.039

fuzzy connectedness, the results of implementing these two algorithms on two images where tumor boundaries are distinct (tumor region with high contrast) and fading and indistinct (tumor region with low contrast) are shown in Fig. 6. In this figure, the images consisting of tumors with distinct and fading boundaries are shown in (a) and (b), respectively. The result of implementing the proposed approach on tumors with distinct boundaries is shown in (c), and (d) shows the segmentation result of the general fuzzy connectedness [24] on this type of tumor (with distinct boundaries). The results of implementing the proposed approach and general fuzzy connectedness [24] on tumor image with fading boundaries are depicted in (e) and (f), respectively.

The mean of validation criteria on image sets and also the total mean achieved from this implementation are provided in Table 3. It is seen from this table that in 50% of the datasets the *SI* criterion is less than 0.7, which shows that the segmentation results are not good [41,42].

Table 4 displays the total means of evaluation criteria in the segmentation methods (general fuzzy connectedness and improved fuzzy connectedness). Criteria values in these two segmentation methods show that performance of the suggested method in all cases is better than that of general fuzzy connectedness. Comparing the two approaches, the proposed approach has on average improved 17.8%, 21.1%, and 6.8% *SI*, *OF*, and *EF* criteria, respectively. In tumors with distinct boundaries, the mean values of criteria corresponding to general fuzzy connectedness are almost acceptable and near to the improved fuzzy

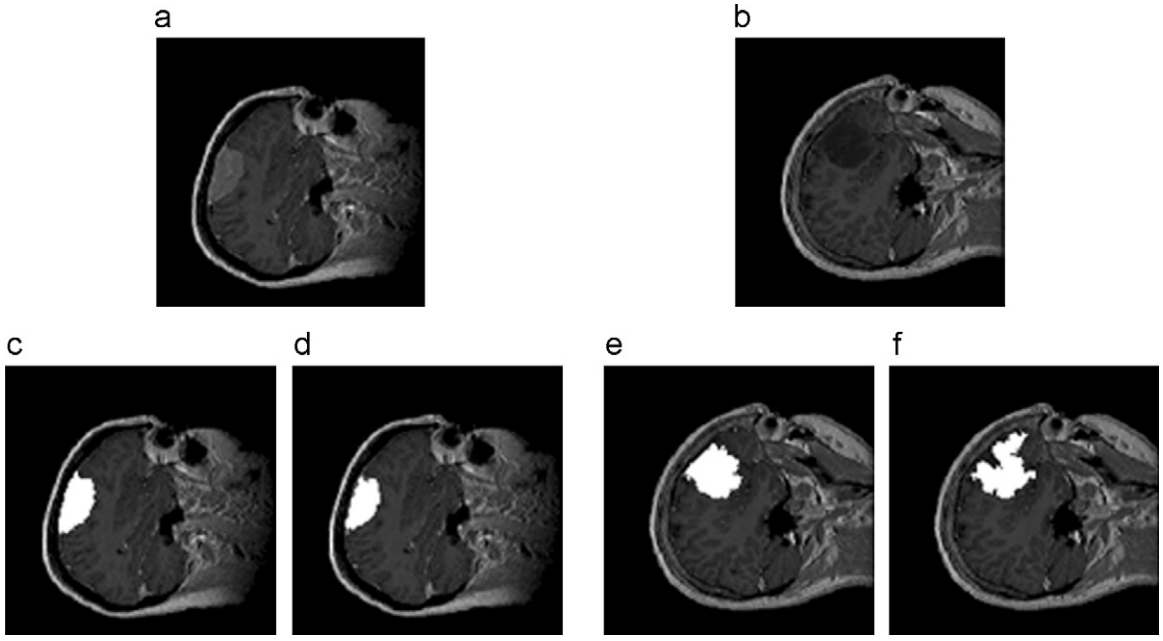

Fig. 6. Comparison between the proposed segmentation algorithm and general fuzzy connectedness on two types of images including tumor with distinct and fading boundaries: (a) input image consists of tumor with distinct boundaries, (b) input image consists of tumor with fading boundaries, (c) segmentation result of tumor with distinct boundaries by proposed approach, (d) segmentation result of tumor with distinct boundaries by general fuzzy connectedness algorithm, (e) segmentation result of tumor with fading boundaries by proposed approach, and (f) segmentation result of tumor with indistinct boundaries by general fuzzy connectedness.

Table 3
Means of criteria (similarity index (*SI*), overlap fraction (*OF*), and extra fraction (*EF*)) with separating image set and for the entire image set (end row), which were calculated by implementing general fuzzy connectedness represented by Udupa and Samarasekera [24].

	SI	*OF*	*EF*
Image set 1	0.90	0.85	0.008
Image set 2	0.83	0.718	0.005
Image set 3	0.694	0.71	0.34
Image set 4	0.835	0.78	0.23
Image set 5	0.64	0.52	0.01
Image set 6	0.523	0.706	0.33
Image set 7	0.97	0.95	0.006
Image set 8	0.60	0.47	0.09
Image set 9	0.55	0.38	0.002
Image set 10	0.96	0.98	0.05
Total means	0.75	0.7064	0.107

Table 4
Total means of criteria in two segmentation methods via improved fuzzy connectedness and general fuzzy connectedness that were represented by Udupa and Samarasekera [24].

	SI	*OF*	*EF*
Improved fuzzy connectedness	0.928	0.917	0.039
General fuzzy connectedness	0.750	0.706	0.107

connectedness results. However in tumors with indistinct boundaries, obvious differences between the corresponding criteria depict robustness of the proposed approach.

The present work can also be compared with some state-of-the-art approach related to the improved generalized fuzzy connectedness such as that of [31]. In that work, the authors evaluated their proposed method using a phantom dataset, and only a few brain lesion MR images, which include distinct boundaries, were considered. However, in the present approach quantification assessment is done at least on 87 MR images of 10 patients with brain tumor. Furthermore, in [31], seed points were selected manually for each image, whereas in the present proposed method seed points are selected automatically, leading to a fully automatic image segmentation approach.

However, due to the dynamic tuning of weights of affinity components as required in the fuzzy connectedness algorithm, the work done in [31], as claimed by the authors, can be applied to various types of images such as MR, CT, and infrared. Whereas, in the present method, since constant optimized weights are used, the method is at present only applicable to brain MR images, and its application for other types of images must be studied.

More features were extracted from tumor texture by feature extraction methods, and their use in automatic seed point selection can be a basis for future studies. On the other hand, changes in the affinity formulations are directly affected in the segmentation results. Combinations of fuzzy connectedness with other methods, especially methods based on the model, can be a strategy for the advancement of this study in the future.

Conflict of interest statement

None declared.

Acknowledgments

The authors would like to thank Drs. Simon Warfield, Michael Kaus, Ron Kikinis, Peter Black, and Ferenc Jolesz for sharing the tumor database on which the algorithm was tested. They would also like to thank Jan Rexilius for his help.

References

[1] L.P. Clarke, R.P. Velthuizen, M. Clark, J. Gaviria, L. Hall, D. Goldgof, R. Murtagh, S. Phuphanich, S. Brem, MRI measurement of brain tumor response: comparison of visual metric and automatic segmentation, Magn. Reson. Imaging 16 (1998) 271–279.

[2] B.N. Joe, M.B. Fukui, C.C. Meltzer, Q. Huang, R.S. Day, P.J. Greer, M.E. Bozik, Brain tumor volume measurement: comparison of manual and semi automated methods, Radiology 212 (1999) 811–816.
[3] M. Vaidyanathan, L.P. Clarke, L.O. Hall, C. Heidtman, R. Velthuizen, K. Gosche, S. Phuphanich, H. Wagner, H. Greenberg, M.L. Silbiger, Monitoring brain tumor response to therapy using MRI segmentation, Magn. Reson. Imaging 15 (1997) 323–334.
[4] M. Vaidyanathan, L.P. Clarke, R.P. Velthuizen, S. Phuphanich, A.M. Bensaid, L.O. Hall, J.C. Bezdek, H. Greenberg, A. Trotti, M. Silbiger, Comparison of supervised MRI segmentation methods for tumor volume determination during therapy, Magn. Reson. Imaging 13 (1995) 719–728.
[5] R.P. Velthuizen, L.P. Clarke, S. Phuphanich, L.O. Hall, A.M. Bensaid, J.A. Arrington, H.M. Greenberg, M.L. Silbiger, Unsupervised measurement of brain tumor volume on MR images, J. Magn. Reson. Imaging 5 (1995) 594–605.
[6] R.P. Velthuizen, L.P. Clarke, L.O. Hall, Feature extraction for MRI segmentation, J. Neuroimaging 9 (1999) 85–90.
[7] L.P. Clarke, R.P. Velthuizen, M.A. Camacho, J.J. Heine, M. Vaidyanathan, L.O. Hall, R.W. Thatcher, M.L. Silbiger, MRI segmentation: methods and applications, Magn. Reson. Imaging 13 (1995) 343–362.
[8] M.C. Clark, L.O. Hall, D.B. Goldgof, R. Velthuizen, R. Murtagh, M.S. Silbiger, Automatic tumor segmentation using knowledge-based techniques, IEEE Trans. Med. Imaging 17 (2) (1998) 187–201.
[9] M. Kamber, R. Shingal, D. Collins, D. Francis, A. Evans, Model-based, 3-D segmentation of multiple sclerosis lesions in magnetic resonance brain images, IEEE Trans. Med. Imaging 6 (1995) 442–453.
[10] A. Zijdenbos, R. Forghani, A. Evans, Automatic quantification of MS lesions in 3D MRI brain data sets: validation of INSECT, Proc. MICCAI (1998) 439–448.
[11] M. Prastawa, E. Bullitt, S. Ho, G. Gerig, A brain tumor segmentation framework based on outlier detection, Med. Image Anal. 8 (2004) 275–283.
[12] D.T. Gering, W.E.L. Grimson, R. Kikinis, Recognizing deviations from normalcy for brain tumor segmentation, in: Medical Image Computing and Computer-Assisted Intervention MICCAI 2002; vol. 2488. Springer, pp. 388–395.
[13] P. Gibbs, D.L. Buckley, S.J. Blackband, A. Horsman, Tumor volume determination from MR images by morphological segmentation, Phys. Med. Biol. 41 (11) (1996) 2437–2446.
[14] M. Kaus, S. Warfield, A. Nabavi, P.M. Black, F.A. Jolesz, R. Kikinis, Automated segmentation of MR images of brain tumors, Radiology 218 (2001) 586–591.
[15] S. Taheria, S.H. Ongb, V.F.H. Chongc, Level set segmentation of brain tumors using a threshold-based speed function, Image Vision Comput. 28 (1) (2009) 26–37.
[16] W.E. Phillips, R.P. Velthuizen, S. Phupanich, L.O. Hall, L.P. Clarke, M.L. Silbiger, Applications of fuzzy C-means segmentation technique for tissue differentiation in MR images of a hemorrhagic glioblastoma multiforme, J. Magn. Reson. Imaging 13 (2) (1995) 277–290.
[17] L.O. Hall, A.M. Bensaid, L.P. Clarke, R. Velthuizen, M. Silbiger, J. Bezdek, A comparison of neural network and fuzzy clustering techniques in segmenting magnetic resonance images of the brain, IEEE Trans. Neural Networks 3 (5) (1992) 672–682.
[18] O. Salvado, P. Bourgeat, O. Tamayo, M. Zuluaga, S. Ourselin, Fuzzy classification of brain MRI using a priori knowledge: weighted fuzzy c-means, MMBIA07 (2007) 1–8.
[19] L. Szilagyi, S. Szilagyi, Z. Benyo, A modified fuzzy c-means algorithm for MRI brain image segmentation, ICIAR07 (2007) 866–877.
[20] A. Rosenfeld, Connectivity in digital pictures, J. Assoc. Comput. Mach. 17 (1970) 146–160.
[21] S. Dellepiane, F. Fontana, Extraction of intensity connectedness for image processing, Pattern Recogn. Lett. 16 (1995) 313–324.
[22] S. Dellepiane, F. Fontana, G.L. Vernazza, Nonlinear image labeling for multivalued segmentation, IEEE Trans. Image Process. 5 (1996) 429–446.
[23] J.K. Udupa, S. Samarasekera, Fuzzy connectedness and object definition, Proc. SPIE: Med. Imaging 2431 (1995) 2–11.
[24] J.K. Udupa, S. Samarasekera, Fuzzy connectedness and object definition: theory, algorithms, and applications in image segmentation, Graph. Models Image Process. 58 (1996) 246–261.
[25] T.N. Jones, D.N. Metaxas, Automated 3D segmentation using deformable models and fuzzy affinity, Proc. Inf. Process. Med. Imaging (1997) 113–126.
[26] T.N. Jones, Image-based Ventricular Blood Flow Analysis, Ph.D. Dissertation, University of Pennsylvania, 1998.
[27] E.D. Angelini, C. Imielinska, Y. Jin, A. Laine, A improving statistics for hybrid segmentation of high-resolution multichannel images, Proc. SPIE: Med. Imaging 4684 (2002) 401–411.
[28] Y. Jin, A. Laine, C. Imielinska, An adaptive speed term based on homogeneity for level-set segmentation, Proc. SPIE: Med. Imaging 4684 (2002) 383–400.
[29] G. Moonis, J. Liu, J.K. Udupa, D.B. Hackney, Estimation of tumor volume with fuzzy-connectedness segmentation of MR images, AJNR Am. J. Neuroradiol. 23 (2002) 356–363.
[30] J.K. Udupa, P.K. Saha, Fuzzy connectedness and image segmentation, Proc. IEEE 91 (10) (2003).
[31] A.S. Pednekar, I.A. Kakadiaris, Image segmentation based on fuzzy connectedness using dynamic weights, IEEE Trans. Image Process. 15 (6) (2006).
[32] J. Hong, Y. Muragaki, R. Nakamura, M. Hashizume, H. Iseki, A neurosurgical navigation system based on intraoperative tumour remnant estimation, J. Robotic Surg. (2007).
[33] M. Kaus, S.K. Warfield, A. Nabavi, P.M. Black, F.A. Jolesz, R. Kikinis, Automated segmentation of MRI of brain tumors, Radiology 218 (2) (2001) 586–591, 〈http://www.spl.harvard.edu/Special:PubDB_View?dspaceid=169〉.
[34] S.K. Warfield, M. Kaus, F.A. Jolesz, R. Kikinis, Adaptive, template moderated, spatially varying statistical classification, Med. Image Anal. 4 (1) (2000) 43–55, 〈http://www.spl.harvard.edu/pages/Software〉.
[35] E. Ardizzone, R. Pirrone, O. Gambino, Automatic segmentation of MR images based on adaptive anisotropic filtering, in: Proceedings of the 12th International Conference on Image Analysis and Processing (ICIAP'03), 2003.
[36] M.S. Atkins, B.T. Mackiewich, Fully automatic segmentation of the brain in MRI, IEEE Trans. Med. Imaging 17 (1) (1998).
[37] J. Canny, A computational approach to edge detection, IEEE Trans. Pattern Anal. Mach. Intell. PAMI-8 (6) (1986) 679–698.
[38] P.K. Saha, J.K. Udupa, D. Odhner, Scale-based fuzzy connected image segmentation: theory, algorithms, and validation, Comput. Vision Image Understanding 77 (2000) 145–174.
[39] A.P. Zijdenbos, B.M. Dawant, R.A. Margolin, A.C. Palmer, Morphometric analysis of white matter lesions in MR images: method and validation, IEEE Trans. Med. Imaging 13 (1994) 716–724.
[40] R. Stokking, K.L. Vincken, M.A. Viergever, Automatic morphology-based brain segmentation (MBRASE) from MRI-T1 data, Neuroimage 12 (2000) 726–738.
[41] J.J. Bartko, Measurement and reliability: statistical thinking considerations, Schizophrenia Bull. 17 (1991) 483–489.
[42] R. Khayati, M. Vafadust, F. Towhidkhah, M. Nabavi, Fully automatic segmentation of multiple sclerosis lesions in brain MR FLAIR images using adaptive mixtures method and Markov random field model, Comput. Biol. Med. 38 (2008) 379–390.

Vida Harati was born in Mashhad, Iran, in 1982. She received an M.Sc. degree from the Shahed University, Iran, in 2009. Her research interests focus on image processing, especially on the methods related to brain tumor segmentation.

Rasoul Khayati was born in Salmass, Iran, in 1966. He received an M.Sc. degree and a Ph.D. degree from the Amirkabir University of Technology, Iran, in 1993 and 2008, respectively. Currently, he is a faculty member of Biomedical Engineering at Shahed University. His research interests focus on biomedical image processing, medical imaging systems, and biological systems modeling.

Abdolreza Farzan was born in Ardakan, Iran, in 1955. He is a neurosurgery specialist in Mostafa Khomeini Hospital, Tehran, Iran. Currently, he is a faculty member of Neurosurgery Department at Shahed University. His research interests focus on different fields of brain tumors, brain trauma, and lumbar disc.